Eur. Phys. J. D (2022) 76:219
https://doi.org/10.1140/epjd/s10053-022-00546-9

THE EUROPEAN PHYSICAL JOURNAL D

Regular Article – Optical Phenomena and Photonics

Dynamics of the Pearcey Gaussian beam in linear potential

Shumin Ren, Teng Guo, Ru Gao, Pengxiang Wang, and Yan Xiao[a]

College of Physics and Electronics Engineering, Shanxi University, Taiyuan 030006, China

Received 22 June 2022 / Accepted 30 October 2022 / Published online 18 November 2022

Abstract. The propagation properties of the Pearcey Gaussian beam based on the fractional Schrödinger equation with linear potential are investigated numerically. It was found that the Pearcey Gaussian beam produces a self-inversion phenomenon due to the effect of the Lévy index from 1 to 2, which is in the absence of the linear potential. The linear potential has a great impact on the transmission path of the Pearcey Gaussian beam from a straight line turn to a zigzag path, and the oscillation period is inversely proportional to the linear potential. Meanwhile, the symbol of the linear potential parameter controls the direction of the incident beam. Moreover, the chirp affects the Pearcey Gaussian beam with an uneven intensity distribution during transmission. These features confirm the promising applications of the Pearcey Gaussian beam in optical manipulation and optical switch.

1 Introduction

In recent years, special light beams exhibit various unique transmission properties in different media, which have attracted the attention of more and more researchers. The Airy beam, as representative of the diffraction-free beams, has self-accelerating and self-healing properties [1]. After this, they continued to study other diffraction-free beams, such as asymmetric Laguerre–Gaussian [2] and the controllable polygon beams [3]. Unlike these beams, the Pearcey beam is the one describing the focal diffraction of a cusp caustic. At the same time, the Pearcey beam exhibits remarkable transmission characteristics such as form-invariance, self-focusing, and self-healing. Due to its special transmission properties, the Pearcey Gaussian beam has attracted an increasing number of researchers to explore its potential for various applications. In 1946, Pearcey used analytical derivation and numerical calculation to research the field structure near the focusing line of cylindrical electromagnetic waves [4] and pushed out the Pearcey beam formula early. In 2012, J.D. Ring applied the Pearcey beam to optics and derived it as form-invariant theoretically and experimentally [5]. In 2015, A.A. Kovalev obtained a new solution of the Schrödinger-type equation which was demonstrated by using the linear combination of two half-Pearcey beams with arbitrary weights, and other form-invariant laser beams can be obtained which are neither full Pearcey beams nor half-Pearcey beams [6]. In 2016, the existence of so-called face-to-face symmetric dual Pearcey beams based on Fresnel diffraction of bright elliptic rings was theoretically proposed and experimentally demonstrated [7]. In 2019, Zang et al. for a one-dimensional Pearcey beam showed that the one-dimensional finite-energy Pearcey beam can be decomposed into two Airy-like beams with opposite acceleration directions, and this acceleration leads to a double self-acceleration behavior of the Pearcey beam, which is of great significance for subsequent experimental studies [8]. Hereafter, a large number of researchers began to invest in the study of the Pearcey beam. A variety of beams derived from the Pearcey integral include symmetric Pearcey Gaussian beam [9], symmetric odd-Pearcey Gaussian beams [10], circular Pearcey beams [11], and elliptical Pearcey beam [12] which have been intensively investigated as well. What is more, there has been a new upsurge in the research on the transmission characteristics and dynamics of Pearcey beams in various potential and mediums, containing harmonic potential [13], parabolic refractive index medium [14, 15], and parabolic potential [16].

A growing chorus of investigations are based on the models of the fractional Schrödinger equation (FSE), and the beam dynamics and manipulations have been investigated extensively. The FSE was derived by Laskin in 2002 [17], which is a generalization of the standard Schrödinger equation by extending the Brownian motion to the Lévy process, and this model can be used to describe fractional field theory and the behavior of fractional spin particles. In 2015, Longhi proposed an optical experiment scheme and introduced the FSE into the field of optics [18], and then this research stimulates interest to investigate the beam propagation in the FSE

[a] e-mail: xiaoyan@sxu.edu.cn (corresponding author)

optical system. In 2016, Wu et al. studied the existence of a soliton-type solution for the fractional Schrödinger equation and proved that the equation has a soliton solution by using a constrained minimization argument [19]. And then, various beams have been studied in FSE theoretical models, such as Gaussian [20] and Airy beam [21], even different media, such as PT-symmetry [22] and linear potential [23]. We have also discussed the input beam that does not carry sidelobes in the linear potential in another study [24]. The input beam studied in this paper can adjust the sidelobe position of the Pearcey Gaussian beam during transmission by setting corresponding parameter values, as [25]. Due to the linear potential, the transmission trajectory of both different forms of Pearcey Gaussian beams will turn into a zigzagging shape. However, without considering the linear potential, the Pearcey Gaussian beam with the sidelobe discussed in this paper has the phenomenon of self-reversal due to the different velocity directions of the sidelobe and main lobe.

2 Theoretical model

In the paraxial approximation, the Pearcey Gaussian beam propagates in the optical system modeled by the FSE with linear potential and is given by:

$$i\frac{\partial\varphi(x,z)}{\partial z}=\frac{1}{2}\left(-\frac{\partial^2}{\partial x^2}\right)^{\alpha/2}\varphi(x,z)+V(x)\varphi(x,z) \tag{1}$$

where $\varphi(x,z)$ is the light field envelope, x and z are the dimensionless transverse coordinate and propagation distance, respectively. And the α is the Lévy index, when $\alpha=2$ Eq. (1) will become a standard Schrödinger equation. $V(x)=\beta x$ is the linear potential. The Fourier transform of Eq. (1) is expressed as [20]:

$$i\frac{\partial\hat{\varphi}(k,z)}{\partial z}=\frac{1}{2}|k|^{\alpha}\hat{\varphi}(k,z)+i\beta\frac{\partial\hat{\varphi}(k,z)}{\partial k} \tag{2}$$

where k is the spatial frequency and the $\hat{\varphi}(k,z)=\int_{-\infty}^{+\infty}\varphi(x,z)e^{-ikx}dx$ is the Fourier transform of $\varphi(x,z)$. And when the $\beta=0$, the solution of Eq. (2) can be written as follows:

$$\phi(x,z)=\frac{1}{2\pi}\int_{-\infty}^{+\infty}\phi_0(k)\exp\left(\frac{-iz|k|^{\alpha}}{2}\right)\exp(ikx)dk \tag{3}$$

The general solution of Eq. (1) with the $\beta\neq 0$ can be given by [22]:

$$\varphi(x,z)=\frac{1}{2\pi}\int_{-\infty}^{+\infty}\varphi_0(k+\beta z)$$

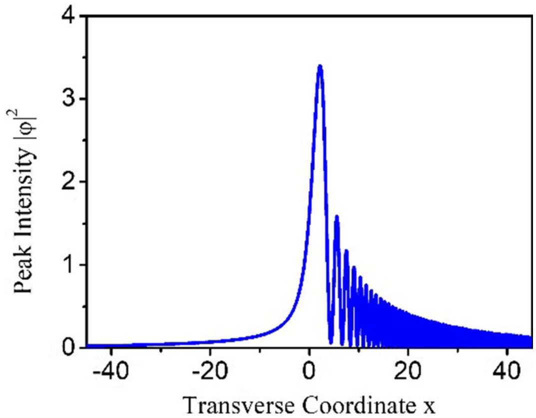

Fig. 1 Initial input beam carries sidelobes, $a=1$ and $b=-1$

$$\exp\left(i\frac{k|k|^{\alpha}-(k+z\beta)|k+\beta z|^{\alpha}}{2\beta(1+\alpha)}\right)\exp(ikx)dk \tag{4}$$

where $\hat{\varphi}_0(k)$ is the Fourier spectrum of the input beam.

Here, the input is chosen as chirp Pearcey Gaussian beam:

$$\varphi(x,0)=Pe(x)\exp(-\chi_0^2x^2)\exp(iCx^2) \tag{5}$$

where C is the chirp parameter, χ_0 is the distribution factor related to the width of the Gaussian function. Like the Airy beam, the Pearcey beam also has infinite energy and can be produced finite by modulating the Pearcey function with the Gaussian function, which does not significantly change the beam's properties.

The Pearcey function expression is defined as:

$$Pe(x)=\int_{-\infty}^{+\infty}\exp[i(as^4+s^2x/b)]ds \tag{6}$$

where a is the coefficient of integral term, and b represents an arbitrary scale factor. Parameters a and b affect the section and phase of the Pearcey function; when the symbols a and b are changed, the profile of the Pearcey function will reverse [23]. In the following, we fixed the $a=1$, $b=-1$. For this paper, the input beam is shown in Fig. 1.

3 Discussion and results

3.1 The case of C = 0

Based on the FSE, the propagation evolution of the Pearcey Gaussian beam with different parameters was obtained by numerical simulation when chirp was not considered.

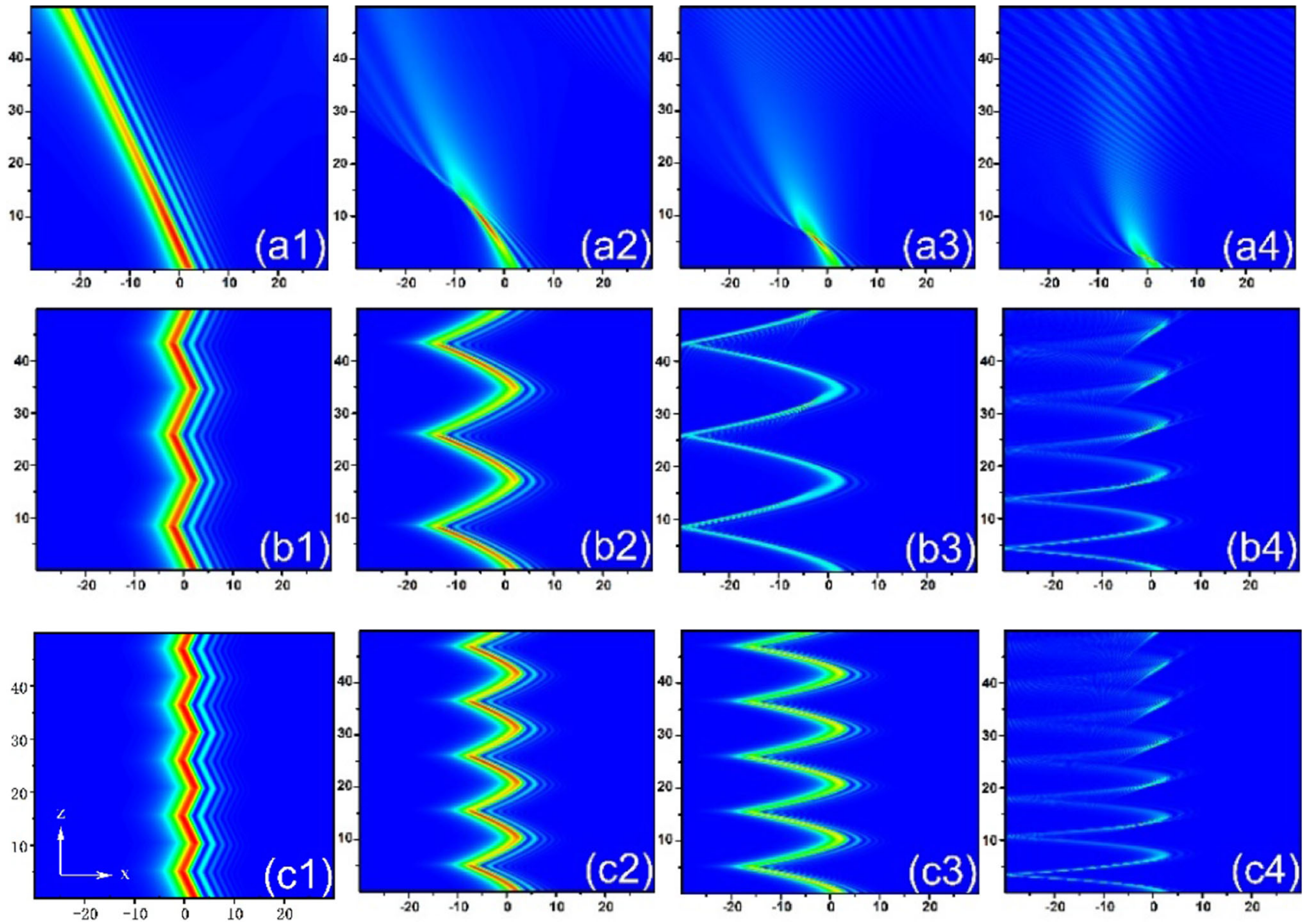

Fig. 2 Propagation evolution of Pearcey Gaussian beam in free space (**a**) and linear potential (**b**, **c**). The linear potential parameters: **a** $\beta = 0$, **b** $\beta = 3$, **c** $\beta = 5$. And Lévy indexes from left to right are 1, 1.4, 1.8, and 2

Figure 2 investigates the effect of the Lévy index on the transmission characteristics of the Pearcey Gaussian beam for different linear potential coefficients. As shown in Fig. 2a1–a4 without linear potential, as the Lévy index increases, the diffraction effect of the beam increases and the beam energy gradually decreases. Then, the Pearcey Gaussian beam begins to gradually reverse as the increase in Lévy index during the transmission. Due to the linear potential, the Pearcey Gaussian beam forms a bound, state and the transmission path oscillates periodically along with a zigzag shape in Fig. 2b1–b4, c1–c4. And from the comparison of Fig. 2b1–b4 and c1–c4, it is clear that the period of the Pearcey Gaussian beam decreases for larger values of the linear potential parameter. In addition, the amplitude of the transverse oscillation of the Pearcey Gaussian beam gradually increases with the increase in the Lévy index, and the enhancement of the diffraction effect leads to the weakening of the beam energy. In Fig. 2b4, c4, the energy of the Pearcey Gaussian beam is weakened, but the transmission period suddenly decreases. In summary, the transmission period of the Pearcey Gaussian beam can be controlled by the value of the linear potential parameter, and the Lévy index has a great influence on the energy intensity in the beam transmission process additionally. According to the characteristics of the beam in the transmission process, it has a certain application value in the optical switch.

The influence of the Lévy index and the linear potential coefficient on the peak intensity of the Pearcey Gaussian beam is further discussed in Fig. 3. By comparing different linear potential parameters (see Fig. 3a), it can be concluded that the peak intensity has approximately the same period when the linear potential coefficients $|\beta|$ are the same. When the linear potential parameter is negative, the peak intensity of the beam during transmission is larger when the linear potential parameter is positive. This is because of the fact that the negative linear potential causes the Pearcey Gaussian beam to gather energy, and the peak intensity becomes stronger. In addition, with the same symbol of linear potential parameter, the larger the linear potential coefficient, the stronger the peak intensity and the smaller the beam transmission period. Figure 3b shows that the Lévy index does not affect the peak intensity oscillation period. With the Lévy index increasing, the oscillation amplitude of the peak intensity becomes larger and larger. The oscillation amplitude reaches the minimum when $\alpha = 1$.

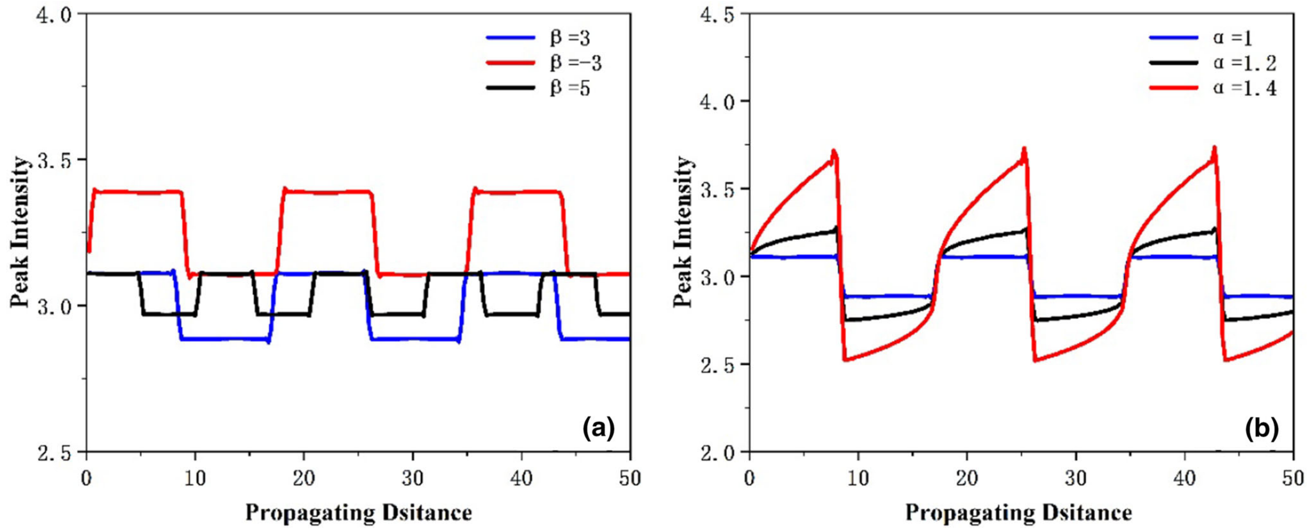

Fig. 3 Peak intensity with the different linear potential parameters β in (**a**) and Lévy index α in (**b**). **a** $\alpha = 1$, **b** $\beta = 3$

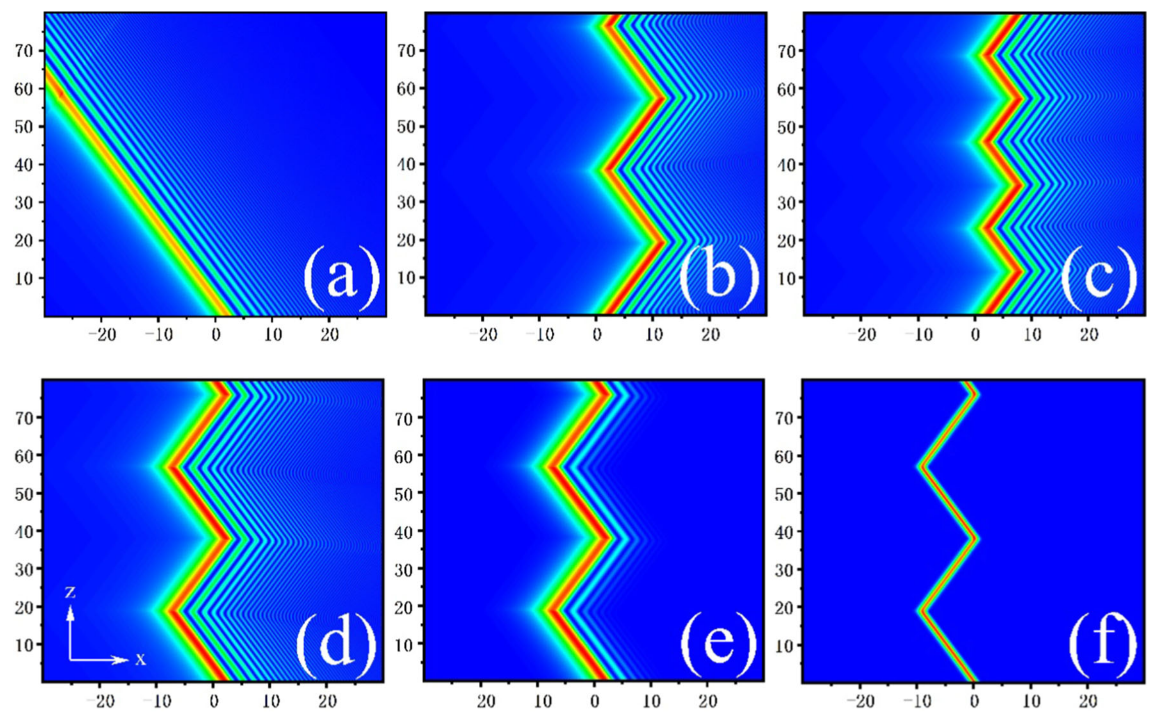

Fig. 4 Propagation evolution of Pearcey Gaussian beam with different linear potential and distribution factors. Lévy index $\alpha = 1$, **a** $\beta = 0$, $\chi_0 = 0.01$, **b** $\beta = -3$, $\chi_0 = 0.01$, **c** $\beta = -5$, $\chi_0 = 0.01$, **d** $\beta = 3$, $\chi_0 = 0.01$, **e** $\beta = 3$, $\chi_0 = 0.1$, **f** $\beta = 3$, $\chi_0 = 1$

The transmission evolution of the Pearcey Gaussian beam under the influence of different distribution factors in linear potential is given in Fig. 4. As shown in Fig. 4 (a-c), the Pearcey Gaussian is accompanied by a large number of sidelobes during transmission with the distribution factor $\chi_0 = 0.01$. When no linear potential is available, the beam transmission proceeds along the straight line in Fig. 4a. Under the influence of the linear potential, the beam transmission forms a bound state and starts along with the z-shape transmission in Fig. 4b, c. The transmission trajectory of the main and sidelobes of the beam is the same, and the capacity is mainly concentrated in the main lobe, respectively. In addition, comparing the evolution results of Fig. 4b, c, the propagation period of the beam increases with the decrease in the linear potential parameter $|\beta|$. Comparing Fig. 4b, d, it is easy to conclude that when the absolute values of the linear potential parameters are the same, the propagation period of the beams is the same. And the linear potential parameter $\beta > 0$, the incident

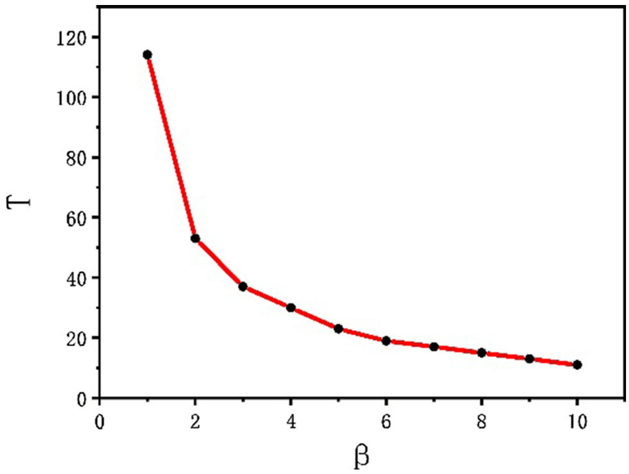

Fig. 5 Effect of linear potential on the period of the Pearcey Gaussian beam. T is the transmission period and is defined as the length of a transmission period

beam is deflected to the left, and vice versa. It can be seen that the symbol of the linear potential parameter does not change the propagation period of the beam but determines the different propagation direction of the initial beam.

When in Fig. 4d–f, the influence on beam transmission is investigated by setting different distribution factors with $\beta = 3$. Since the distribution factor determines the width of the Gaussian function, the number of sidelobes of the beam can be controlled during the transmission. Therefore, in Fig. 4e, f, the number of sidelobes gradually decreases as the distribution factor increases, and the sidelobe disappears completely when $\chi_0 = 1$.

To further study the influence of linear potential on the beam transmission period, Fig. 5 visualizes the relationship between linear potential and beam transport period which decreases as the linear potential parameter increases, and it is consistent with the findings in Figs. 2 and 4 above. In addition, the curve shows a fast downward trend in the early stage and a flat trend in the later stage. Therefore, the period evolution of the beam can be controlled by changing the linear potential parameter.

3.2 The case of $C \neq 0$

Herein, we investigate the evolution of the initially chirped Pearcey Gaussian beam with different linear potential parameters, and the results are shown in Figs. 6, 7.

In Fig. 6a3, the initial Pearcey Gaussian beam propagates along a straight line with sidelobe on the left when the effect of chirp is not considered. Additionally,

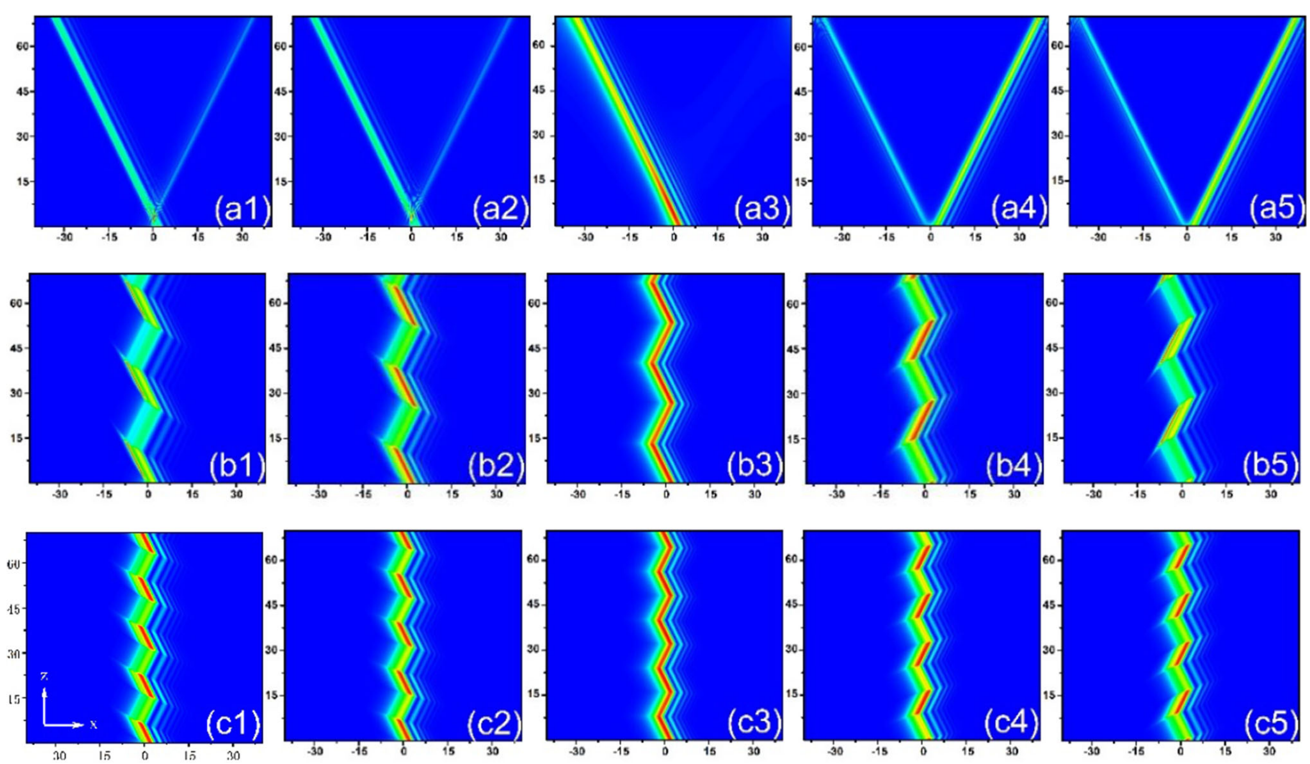

Fig. 6 Transmission evolution of the Pearcey Gaussian beam with chirp. Lévy index α=1, linear potential parameters: **a** $\beta = 0$, **b** $\beta = 3$, **c** $\beta = 5$, distribution factor $\chi_0 = 0.1$. And the chirp parameters C from left to right are − 1.2, − 0.8, 0, 0.8, and 1.2

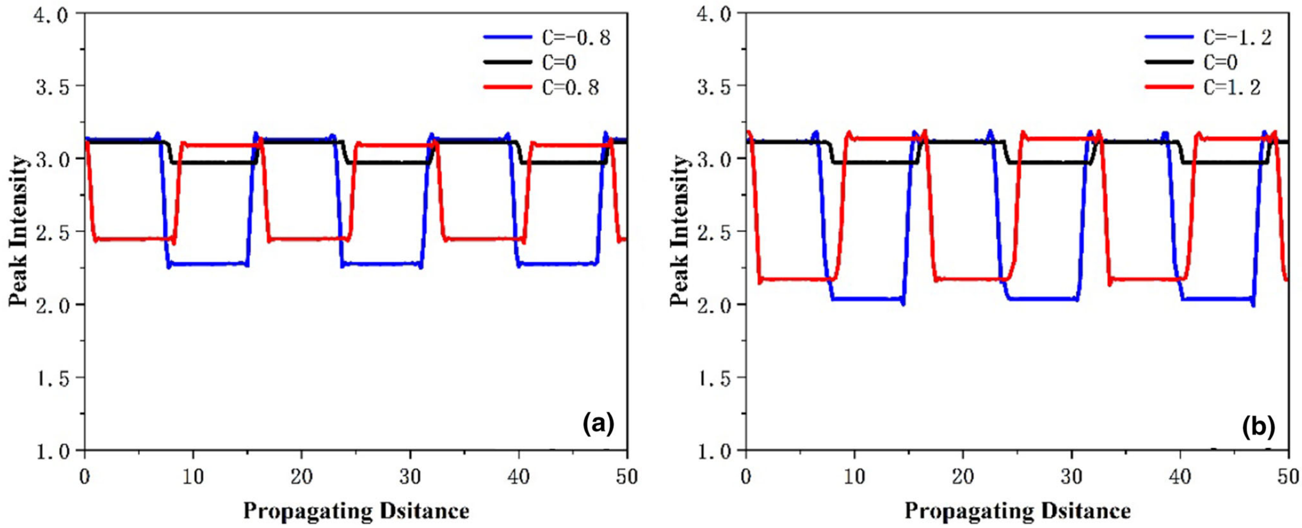

Fig. 7 Peak intensity of the Pearcey Gaussian beam with chirp. **a** Chirp parameters $C = -0.8, 0, 0.8$, **b** Chirp parameters $C = -1.2, 0, 1.2$

the transmission direction of the sidelobe is the same as that of the main lobe, and the main energy of the beam is concentrated on the main lobe of the beam and the direction of the sidelobe in the direction of the main lobe. Due to the positive chirp, the main lobe and the sidelobe propagate in opposite directions, as shown in Fig. 6a4, a5, where the main lobe of the beam starts to propagate in a straight line in the right direction. The negative chirp is the exact opposite of the positive chirp. In Fig. 6a1, a2 the main lobe transmits in the left direction and the sidelobe in the right direction, and both plots also show that the beam has traveled a short distance before splitting.

When the beam is transmitted with the linear potential, the Pearcey Gaussian beam no longer splits but is transmitted in the shape of a zigzag periodically. In Fig. 6b3, c3, the beam has an essentially uniform distribution during transmission. However, in each cycle, the first half of the energy is weakened and the second half is strengthened when $C > 0$ in Fig. 6b4, b5, c4, c5. While $C < 0$, the trend is reversed with positive chirp, the beam intensity at the former half of one period always gets enhanced and the latter half of one period always diminishes in Fig. 6b1, b2, c1, c2. In addition, the light intensity becomes weaker as the absolute value of the chirp parameter increases (see Fig. 6b1, b5). This phenomenon diminishes when the effect of the linear potential is larger, compared to Fig. 6b1 with Fig. 6c1, b5 with Fig. 6c5. Taken together, the sign of the linear potential parameter determines the direction of the input beam, while the chirp affects the energy distribution of the beam.

To further investigate the effect of the initial chirped Pearcey Gaussian beam on the propagation evolution, Fig. 7 plots the variation of the peak intensity of the beam during the propagation process. Comparing the two sets of Fig. 7a, b, it can be intuitively concluded that the larger the chirp, the lower the peak intensity. Both figures show that in the absence of chirp, the energy of the beam is almost uniformly distributed, but the intensity of the beam in the second half of a period is always enhanced with the positive chirp parameter; in the first half of a period, the negative chirp parameter is enhanced. In addition, the peak intensity maxima at positive and negative chirps are essentially the same. This is consistent with the findings in Fig. 6. Therefore, chirp can control the energy of the beam well and has important applications for beam control.

4 Conclusions

In this paper, the dynamics of Pearcey Gaussian beams in the fractional Schrödinger equation with linear potential are studied. As the Lévy index increases, the Pearcey Gaussian beam produces self-reflection phenomena without linear potential, and the diffraction effect increases. When the linear potential is considered, the transmission path of the Pearcey Gaussian beam has a zigzag shape, and the diffraction effect increases with the increase in the Lévy index. The oscillation period of the Pearcey Gaussian beam decreases with the increase in the linear potential, and the symbol of the linear potential parameter determines the propagation direction of the initial beam. The negative chirp parameter always enhances the intensity of the beam in the first half-period, while the positive chirp parameter always enhances the intensity of the beam in the second half-period. The higher the absolute value of the chirp parameter, the lower the peak intensity. These properties have potential applications in optical switching and optical control.

Author contribution

SR involved in formal analysis, validation, data curation, writing–original draft, and visualization. TG involved in formal analysis and validation. RG involved in formal analysis and validation. PW involved in formal analysis, validation, and supervision. YX involved in conceptualization, methodology, formal analysis, validation, supervision, and writing–review and editing.

Data Availability Statement This manuscript has associated data in a data repository. [Authors' comment: All data generated or analysed during this study are included in this published article.]

Declarations

Conflict of interest No potential conflict of interest was reported by the authors.

References

1. W.P. Zhong, W.Y. Zhong, M. Belić, Z.P. Yang, Optik **245**, 167612 (2021)
2. W.P. Zhong, W.Y. Zhong, M. Belić, Z.P. Yang, Phys. Lett. A **423**, 127818 (2022)
3. W.P. Zhong, W.Y. Zhong, M. Belić, Z.P. Yang, Phys. Lett. A **432**, 128009 (2022)
4. T. Pearcey, Philos. Mag. **137**(268), 311–317 (1946)
5. J.D. Ring, J. Lindberg, A. Mourka, A. Mourka, M. Mazilu, K. Dholakia, M.R. Dennis, Opt. Express **20**(17), 18955–18966 (2012)
6. A.A. Kovalev, V.V. Kotlyar, S.G. Zaskanov, A.P. Porfirev, J. Opt. **17**, 035604 (2015)
7. Z. Ren, C. Fan, Y. Shi, B. Chen, J. Opt. Soc. Am. A **33**(8), 1523–1530 (2016)
8. F. Zang, W. Yan, L. Li, Results Phys. **15**, 102656 (2019)
9. Y. Wu, Y. Wu, J. Zhao, Z. Lin, H. Huang, C. Xu, Y. Liu, K. Chen, X. Fu, H. Qiu, H. Liu, G. Wang, X. Yang, D. Deng, L. Shui, Opt. Lett. **46**(10), 2461–2464 (2021)
10. K. Zhou, S. He, S. Hong, Y. Wu, D. Deng, J. Guo, Results Phys. **19**, 103526 (2020)
11. L. Zhang, S. He, X. Peng, L. Huang, X. Yang, G. Wang, H. Liu, Y. He, D. Deng, Chaos, Solitons Fractals **143**, 110608 (2021)
12. J. Jiang, Z. Mo, D. Xu, H. Huang, L. Zhang, H. Yang, H. Huang, Y. Wu, L. Shui, H. Liu, D. Deng, Opt. Cmm. **504**, 127475 (2022)
13. J. Wu, C. Xu, L. Wu, D. Deng, Opt. Comm. **478**, 126367 (2021)
14. C. Xu, J. Wu, Y. Wu, L. Lin, J. Zhang, D. Deng, Opt. Comm. **464**, 125478 (2020)
15. Z. Lin, Y. Wu, H. Qiu, X. Fu, K. Chen, D. Deng, Commun. Nonlinear Sci. **94**, 105557 (2021)
16. Z. Lin, C. Xu, H. Huang, Y. Wu, H. Qiu, X. Fu, K. Chen, X. Yu, D. Deng, Opt. Express **29**(11), 16270–16283 (2021)
17. N. Laskin, Phys. **66**, 056108 (2002)
18. L. Stefano, Opt. Lett. **40**(6), 1010–1013 (2015)
19. Q. Li, X. Wu, Appl. Math. Lett. **53**, 119–124 (2016)
20. F. Zang, Y. Wang, L. Li, Opt. Express **26**(18), 23740–23750 (2018)
21. X. Huang, Z. Deng, X. Fu, J. Opt. Soc. Am. B **34**(5), 976–982 (2017)
22. Y. Zhang, H. Zhong, M.R. Belić, Y. Zhu, W. Zhong, Y. Zhang, M. Xiao, Laser Photonics Rev. **10**(1), 3–9 (2016)
23. A. Liemert, A. Kienle, Math. **4**(31) (2016)
24. S. Ren, R. Gao, T. Guo, P. Wang, Y. Xiao, J. Phys. B: At. Mol. Opt. Phys. **55**, 205401 (2022)
25. F. Zang, L. Liu, F. Deng, Y. Liu, L. Dong, Y. Shi, Opt. Express **29**(16), 26048–26057 (2021)